



**HAL**  
open science

## Hydroxyapatite as a new support material for cobalt-based catalysts in Fischer-Tropsch synthesis

Rajesh Munirathinam, Doan Pham Minh, Ange Nzihou

### ► To cite this version:

Rajesh Munirathinam, Doan Pham Minh, Ange Nzihou. Hydroxyapatite as a new support material for cobalt-based catalysts in Fischer-Tropsch synthesis. *International Journal of Hydrogen Energy*, 2020, 45 (36), pp.18440-18451. 10.1016/j.ijhydene.2019.09.043 . hal-02304588

**HAL Id: hal-02304588**

**<https://imt-mines-albi.hal.science/hal-02304588>**

Submitted on 3 Oct 2019

**HAL** is a multi-disciplinary open access archive for the deposit and dissemination of scientific research documents, whether they are published or not. The documents may come from teaching and research institutions in France or abroad, or from public or private research centers.

L'archive ouverte pluridisciplinaire **HAL**, est destinée au dépôt et à la diffusion de documents scientifiques de niveau recherche, publiés ou non, émanant des établissements d'enseignement et de recherche français ou étrangers, des laboratoires publics ou privés.

# Hydroxyapatite as a new support material for cobalt-based catalysts in Fischer-Tropsch synthesis

MunirathinamRajesh<sup>a,\*</sup>, Doan Pham Minh<sup>a,b</sup>, Nzihou Ange<sup>a</sup>

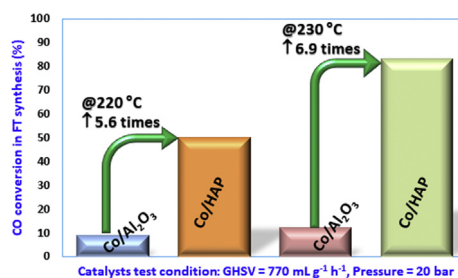
<sup>a</sup> Université de Toulouse, IMT-Mines Albi, UMR CNRS 5302, Centre RAPSODEE, Campus Jarlard, F-81013 Albi Cedex 09, France

<sup>b</sup> Institute of Research and Development, Duy Tan University, Da Nang 550000, Viet Nam

## HIGHLIGHTS

- HAP as a catalyst support material was studied in FT synthesis for the first time.
- HAP support material exhibited lower acid-site density than alumina support.
- Co<sub>3</sub>O<sub>4</sub> particles were easier to reduce when supported on HAP than on alumina.
- Co/HAP exhibited higher CO conversion than Co/alumina catalysts.

## GRAPHICAL ABSTRACT



## ABSTRACT

Hydroxyapatite [HAP, (Ca<sub>10</sub>(PO<sub>4</sub>)<sub>6</sub>(OH)<sub>2</sub>)] is an emerging catalytic support possessing exciting features such as high thermal and mechanical strength, chemically stable with low water solubility along with tunable porosity and acid-basic character. Despite of these interesting characteristics, it has not yet been investigated in Fischer-Tropsch (FT) synthesis. Herein, for the first time, HAP-supported cobalt catalysts (Co/HAP) prepared by conventional incipient wetness impregnation method were examined in the FT synthesis process. The catalytic performance of these catalysts was compared with alumina-supported cobalt catalysts (Co/Alumina). HAP support was found to exhibit considerably less acid-site density, consequently, reducing detrimental interactions of the support with cobalt precursors leading to hardly reducible Co species that are generally observed with its alumina counterpart. Co/HAP catalysts exhibit relatively larger Co particle sizes (~9 nm versus ~6 nm, as observed from TEM analysis) and better Co reducibility when compared to its counterparts on alumina. FT synthesis at 20 bar, 220 °C and H<sub>2</sub>/CO = 2.1 showed that the CO conversion was higher on the catalysts (10 wt% Co loading) using HAP as a support material when compared to alumina. Under different testing conditions (220 or 230 °C)

Keywords:

Hydroxyapatite

Fischer-Tropsch synthesis

Supported cobalt catalyst

Alumina

\* Corresponding author.

E-mail address: [rajesh.munirathinam@mines-albi.fr](mailto:rajesh.munirathinam@mines-albi.fr) (R. Munirathinam).

using the Co/HAP catalyst, the C<sub>5+</sub> selectivity was in the range of 82–88%, whereas the methane selectivity was about ~10%.

---

## Introduction

Growing global awareness for decreasing heavy reliance on petroleum reserves to produce transportation fuels and value-added chemicals has called for the renewed interest in both academia and industry towards Fischer-Tropsch (FT) synthesis [1,2]. FT synthesis is a heterogeneous catalytic process that uses synthesis gas (syngas, CO + H<sub>2</sub>) to produce liquid hydrocarbon fuels, along with alkenes and oxygenates. Syngas originates from non-petroleum feedstocks such as coal, natural gas, biomass and other materials rejected as wastes [3,4]. Mounting interest to valorize biomass and wastes for sustainable environment has augmented the production of syngas, which can be further processed by FT synthesis to produce value added biofuels [5,6].

FT catalysts generally consist of either cobalt or iron nanoparticles, which are dispersed on support materials such as alumina, silica, zirconium oxide, titanium oxide, niobium oxide, carbon or SiC. Cobalt-based catalysts favor the synthesis of high-molecular weight hydrocarbons (paraffin wax) that can be further hydrocracked to yield diesel fuels and lubricants [2,7], whereas, iron-based catalysts exhibit the formation of lower olefins, which can be further processed to produce products such as polymers, solvents and drugs [8]. Generally, ideal mesoporous supports provide thermal, mechanical, and chemical stability, further, its high specific surface area and specific pore volume lead to facile catalyst preparation, better mass transfer characteristics, and high metal (active phase) dispersion [9,10].

Interaction between support material and metallic precursor plays a crucial role in determining the active phase dispersion [11]. For e.g. strong interaction between alumina and silica with cobalt species favors high Co dispersion, however, this phenomenon leads to the formation of small Co nanoparticles and refractory species, namely, Co aluminates or Co silicates, that are hard to reduce [12,13]. On the contrary, weakly interacting supports like carbon-based materials give rise to poor dispersion, and thus a low ratio of surface Co metal sites [14]. Therefore, a trade-off must be found. In the direction of improving support characteristics, structural promoters belonging to transition metal oxides, namely, zirconia, chromia or manganese oxides, and some rare earth metal oxides, namely, lanthanide, ceria, or thorium oxide are sometimes added to conventional supports like alumina, silica, or titania to enhance the active phase dispersion and its stability, subsequently, leading to improved performance in FT synthesis [15]. Mesoporous periodic silicas (MCM41 and SBA-15) are another group of model catalytic supports with tailored

pore size distributions that enable to study their effect in FT synthesis [16,17]. Zeolites are crystalline microporous aluminosilicates-based support material with tunable surface acid sites upon impregnation with cobalt metal precursor serve as bifunctional catalyst composition in which metallic cobalt produces long-chain hydrocarbons that subsequently reacts at the zeolite acid sites to yield a more branched hydrocarbons of limited chain length and aromatics [18,19]. FT synthesis is an exothermic process, therefore thermal exchange capacity of the support material is of primary importance. Owing to the superior thermal exchange characteristics, coupled with chemical stability of SiC compared with conventional oxide support, SiC is applied as a support material for FT catalysts and found to exhibit high selectivity to long-chain hydrocarbons in FT synthesis [20,21]. Despite of these developments on catalyst support materials, still there is a need to find promising new catalytic support materials with easily tunable acid-base character with high thermal, mechanical and chemical stability to be applied in FT synthesis.

Hydroxyapatite (HAP, Ca<sub>10</sub>(PO<sub>4</sub>)<sub>6</sub>(OH)<sub>2</sub>), a chief component of animal bones and teeth, belongs to the apatite family, has already demonstrated its utility in chemical and materials industry. In addition, HAP is increasingly gaining attention both as the catalyst and the support material [22–24]. It contains both acid and basic sites in its crystal lattice helping to serve as a catalyst, for e.g. in the synthesis of valuable compounds such as 1-butanol and 1,3-butadiene from ethanol [25]. The molar (stoichiometric) ratio of Ca/P in HAP is 1.67 and by varying this molar ratio, the acid-base sites can be tuned yielding nonstoichiometric and yet stable HAP. Further, the structure of HAP is flexible to both cationic (i.e. Ca<sup>2+</sup> ions by Sr<sup>2+</sup>, Mg<sup>2+</sup>, Na<sup>+</sup>, K<sup>+</sup>, etc.) and anionic (i.e. OH<sup>-</sup> ions by F<sup>-</sup>, Cl<sup>-</sup>, CO<sub>3</sub><sup>2-</sup> and/or PO<sub>4</sub><sup>3-</sup> anions by CO<sub>3</sub><sup>2-</sup>, HPO<sub>4</sub><sup>2-</sup>, VO<sub>4</sub><sup>3-</sup>, etc.) substitutions providing additional parameter to control surface acid-basic character and morphology [26,27]. Furthermore, HAP owns vital catalytic support material properties such as tunable specific surface area with or without mesopores, high thermal (~800 °C) and mechanical stability, and very low water solubility [28–30]. Leveraging these support characteristics, recently, we have reported the catalytic activity and stability of HAP supported catalysts in dry reforming of methane [31,32]. These observations about HAP support has prompted us to prepare HAP-supported cobalt catalysts and evaluate its performance for the first time in FT synthesis. To begin with cobalt was chosen as a FT catalyst in this study owing to its high selectivity to long-chain hydrocarbons.

## Experimental section

### Materials

All the chemicals were purchased from Alfa Aesar and used as received, unless specified. Alumina ( $\gamma$ -Al<sub>2</sub>O<sub>3</sub>, PuralNW) and hydroxyapatite (HAP) supports were provided by SASOL and PRAYON S. A. (Belgium), respectively. In brief, HAP preparation is carried out by simultaneous addition of Ca(OH)<sub>2</sub> and H<sub>3</sub>PO<sub>4</sub> in the stirred tank reactor resulting in a precipitate that is eventually washed thoroughly with water and dried to yield HAP. Distilled water was used in the catalyst preparation protocol. The gases used were of high purity (>99%) supplied by Linde.

### Catalyst preparation

Supported-cobalt catalysts, namely, Co/ $\gamma$ -Al<sub>2</sub>O<sub>3</sub> and Co/HAP, with 10 wt% loading of cobalt were prepared by incipient wetness impregnation method. Co(NO<sub>3</sub>)<sub>2</sub>·6H<sub>2</sub>O dissolved in water was used as a catalyst precursor. The solution containing predetermined quantity of cobalt was contacted with a dry support and left for maturation at room temperature for 2 h. Then, the catalysts were dried in an oven maintained at 60 °C under static air for 16 h, followed by calcination at 350 °C in static air for 3 h using a heating rate of 1 °C min<sup>-1</sup>. Thus obtained catalysts 10 wt%Co/ $\gamma$ -Al<sub>2</sub>O<sub>3</sub> and 10 wt%Co/HAP, would henceforth be denoted as Co/Al<sub>2</sub>O<sub>3</sub> and Co/HAP, respectively. Table 1 summarizes the catalysts prepared, where the targeted metal content was 10 wt% of cobalt metal in each catalyst.

### Catalysts characterization

Textural, elemental (ICP-OES), XRD, TPR, TPD and transmission electron microscopy (TEM) analyses were performed as described below.

#### Textural analysis

N<sub>2</sub> adsorption isotherms were recorded to determine the textural properties of the support and the calcined catalyst by means of a Micromeritics Tristar II 3020. BET surface area was calculated from the nitrogen adsorption isotherms in the P/P<sub>0</sub> range from 0.05 to 0.20. Before the analysis, the sample was degassed at 105 °C for 24 h at low pressure (<50 mbar). BJH method was used to calculate the pore size distributions. The BET surface area (S<sub>BET</sub>), specific pore volume, and pore diameter are presented in Table 1.

#### ICP-OES analysis

Inductively coupled plasma-optical emission spectroscopy (ICP-OES) analysis was performed to determine the cobalt content in the catalysts using a HORIBA Jobin Yvon Ultima 2 apparatus. Before the measurements, 5 mL of aqua regia (33 vol% HNO<sub>3</sub> + 67 vol% HCl) was used to dissolve 100 mg of the HAP-supported cobalt catalysts and heated at 90 °C for 1 h and then diluted to 50 mL. 5 mL of HCl (67 vol%) was used to dissolve 100 mg of the Al<sub>2</sub>O<sub>3</sub>-supported cobalt catalysts and heated at 220 °C in the autoclave for 14 h and then diluted to 50 mL.

#### XRD analysis

X-ray diffraction (XRD) measurements were carried out on supports and calcined catalysts by means of a Phillips Panalytical X'pert Pro MPD diffractometer functioning with Cu K $\alpha$  radiation ( $\lambda = 1.543 \text{ \AA}$ ) over a  $2\theta$  range of 10–75° with scan step size of 0.042° s<sup>-1</sup> and a nickel filter to suppress the Cu K $\beta$  ray. International Centre for Diffraction Data (ICDD) database was used to compare the diffraction patterns of our samples with standard patterns. Average Co<sub>3</sub>O<sub>4</sub> nanocrystallite size was calculated from the Debye-Scherrer-equation using the diffraction peak located at  $2\theta = 36.9^\circ$  [33].

#### TPR analysis

Temperature-programmed reduction (TPR) profiles of the calcined catalysts were recorded in the temperature range of 40–1000 °C using a Micromeritics AutoChem 2920 Analyzer. 100 mg of the sample was placed in a quartz reactor and reduced by a 5% H<sub>2</sub>/N<sub>2</sub> gas mixture with a flow rate of 25 mL min<sup>-1</sup> and a heating rate of 10 °C min<sup>-1</sup>. Before the analysis, the sample was purged under the atmosphere of pure helium at 120 °C for 60 min to clean the surface of the sample.

#### TPD analysis

Ammonia temperature-programmed desorption (NH<sub>3</sub>-TPD) were performed to evaluate the acidity of the samples using Micromeritics AutoChem 2920 Analyzer fitted with a thermal conductivity detector (TCD). 100 mg of the support material was pretreated at 400 °C (10 °C min<sup>-1</sup>) for 2 h under helium flow (50 mL min<sup>-1</sup>) and then it was cooled to 100 °C. Then, the sample was saturated with 5% NH<sub>3</sub>/He (50 mL min<sup>-1</sup>) for 60 min. Later, 50 mL min<sup>-1</sup> flow of He was flushed for 60 min to remove physisorbed NH<sub>3</sub> molecules and the TCD detector was let to reach a stable baseline. Finally, TPD of chemisorbed NH<sub>3</sub> molecules was recorded from 100 to 400 °C at a heating rate of 10 °C min<sup>-1</sup>.

**Table 1 – Weight percentage of Co in the calcined catalyst and textural properties of the supports and catalysts.**

Supports/Catalysts	Targeted Co weight percentage	Measured Co weight percentage	S <sub>BET</sub> (m <sup>2</sup> g <sup>-1</sup> )	Specific pore volume (cm <sup>3</sup> g <sup>-1</sup> )	Pore diameter (nm)	Acid site density ( $\mu\text{mol m}^{-2}$ )
HAP	–	–	65	0.33	20 <sup>a</sup>	1.5
Al <sub>2</sub> O <sub>3</sub>	–	–	126	0.27	8	10.6
Co/HAP	10	9.0	48	0.27	22 <sup>a</sup>	
Co/Al <sub>2</sub> O <sub>3</sub>	10	9.6	112	0.21	7	

<sup>a</sup> Broad pore size distribution was observed which is depicted in Fig. S1 of the supporting information.

### TEM-EDX analysis

Bright field transmission electron microscopy (TEM) and high angle annular dark field (HAADF) STEM imaging were performed on the calcined and spent catalysts recovered after catalytic tests using a FEG JEOL JEM 2100F microscope coupled with a field emission gun operated at 200 keV and EDX detector. The supported catalysts were crushed into a fine powder and a small amount of it was dispersed in ethanol and ultrasonicated for few minutes. Two drops of thus prepared solution were drop casted on a carbon coated copper grid and the solvent was let to evaporate, after which the samples were placed in a sample holder for TEM analysis. For each sample, at least 250 cobalt particles have been counted in order to obtain average particle size.

### Catalytic test

The catalysts were evaluated in Fischer-Tropsch synthesis in a fixed bed reactor (TOP Industries) with inner diameter of 14.4 mm, filled with 3 g of the catalyst diluted with 12 g of SiC (to improve the heat exchange inside the catalyst bed) at the middle section of the reactor and the remaining portion of the reactor was filled with inert alumina. The schematic diagram of the fixed-bed reactor used in this study is shown in Fig. 1. The temperature of the reactor was measured and controlled with the help of a thermocouple placed at the center of the catalyst bed. The calcined catalyst was reduced *in situ* at the set temperature (350 or 400 °C) for 7 h or 16 h under 40% H<sub>2</sub>/Ar flow (100 mL min<sup>-1</sup>). After this reduction step, the FT synthesis reaction was conducted at the set temperature (220 or 230 °C) and a syngas (diluted with 25% argon) pressure of 20 bar with varying space velocities (1540/770 mL h<sup>-1</sup> g<sub>cat</sub><sup>-1</sup>) and at a constant H<sub>2</sub>/CO ratio of 2.1. Back pressure regulator was used to set the predetermined pressure during the FT synthesis. Gas meter was used at the outlet of the reactor to measure the gas flow rate before and during the catalytic test. The conversion of CO was calculated using the following expression:

$$\text{CO conversion(\%)} = \left( \frac{\dot{Q}_{(\text{CO})\text{in}}}{\dot{Q}_{(\text{Ar})\text{in}}} - \frac{\dot{Q}_{(\text{CO})\text{out}}}{\dot{Q}_{(\text{Ar})\text{out}}} \right) / \left( \frac{\dot{Q}_{(\text{CO})\text{in}}}{\dot{Q}_{(\text{Ar})\text{in}}} \right) * 100 \quad (1)$$

where  $\dot{Q}_{(\text{CO})\text{in}}$  and  $\dot{Q}_{(\text{CO})\text{out}}$  are the CO molar flow rates (mmol h<sup>-1</sup>) at the inlet and outlet of the reactor and  $\dot{Q}_{(\text{Ar})\text{in}}$  and  $\dot{Q}_{(\text{Ar})\text{out}}$  are the molar flow rates (mmol h<sup>-1</sup>) at the inlet and outlet of the reactor. The product selectivity (S) in FT synthesis to the lower hydrocarbon fractions (C<sub>1</sub>-C<sub>4</sub>) and products with five and more carbons (C<sub>5+</sub>) were calculated from CO conversion and the corresponding yields (Y) were calculated from the following expressions 2 and 3:

$$S_{\text{CX}} = Y_{\text{CX}} / \left( \dot{Q}_{(\text{CO})\text{in}} - \dot{Q}_{(\text{CO})\text{out}} \right) \quad (2)$$

$$S_{\text{C5+}} = 1 - S_{\text{C1-C4}} \quad (3)$$

The liquid products were condensed in cold condenser (maintained at 5 °C) and the components in the gas phase at

the outlet of the reactor were quantified using an Agilent μ-GC A3000 coupled with a TCD.

---

## Results and discussion

### Preparation and characterization of cobalt catalysts supported on HAP and alumina

HAP-supported cobalt catalyst with 10 wt% metal loading (Co/HAP) was prepared by incipient-wetness impregnation method as described in the experimental section. Since alumina is a well-established catalyst support applied in industry, alumina-supported cobalt catalyst (Co/Alumina) was also prepared in order to compare the efficiency of both the catalysts in FT synthesis. HAP support contains both meso- and macropores (Fig. S1) with a mean diameter of 20 nm and a specific surface area of 65 m<sup>2</sup> g<sup>-1</sup>, whereas, alumina contains only mesopores (Fig. S2) with a mean diameter of 8 nm and a specific surface area of 126 m<sup>2</sup> g<sup>-1</sup> (Table 1). As expected, the surface area per gram of both the calcined catalysts, Co/HAP and Co/Alumina, decreased with respect to the bare support (Figs. S1-2). NH<sub>3</sub>-TPD analysis showed that HAP support (1.5 μmol m<sup>-2</sup>) possesses very low acid-site density when compared to that on alumina (10.6 μmol m<sup>-2</sup>). Further, in case of HAP only weak acidic sites were present, whereas, in case of alumina, in addition to weak acidic sites a significant amount of moderate to strong acidic sites were also present (Fig. S3). The differences in the number of acid-site density between HAP and alumina might conceivably change their interaction with the cobalt metal precursor.

XRD patterns of both the supports (HAP and alumina) and the calcined catalysts (Co/HAP and Co/Alumina) are presented in Fig. 2. After the calcination step, Co<sub>3</sub>O<sub>4</sub> was the only detected Co phase on both Co/HAP and Co/Alumina catalysts. However, the presence of mixed cobalt-support oxides phase and other cobalt oxide phases (CoO, Co<sub>3</sub>O<sub>4-x</sub>) cannot be ruled out as they are usually amorphous in nature and do not pro-

---

duce any distinct XRD patterns. Further, XRD technique is not very sensitive in detecting the presence of such small amorphous cobalt oxide crystallites (~3 nm) [2]. The intensity of the XRD patterns in Co/HAP is slightly higher than that of bare HAP indicating increased crystallinity of HAP phase, owing to the thermal treatment during the calcination step.

Co<sub>3</sub>O<sub>4</sub> crystallite sizes in the Co/HAP and Co/Alumina catalysts were calculated from the Co<sub>3</sub>O<sub>4</sub> peak at 36.9° (2θ) using the Debye-Scherrer-equation and are shown in Table 2 [33]. Co<sub>3</sub>O<sub>4</sub> crystallites were bigger in size on HAP (12.2 nm) than on alumina (9.4 nm) which can be visually conceived from the intensity of XRD patterns of Co<sub>3</sub>O<sub>4</sub> phase on the corresponding support (Fig. 2).

The average Co<sub>3</sub>O<sub>4</sub> particle size was also obtained from the statistical treatment of the TEM images and is presented in



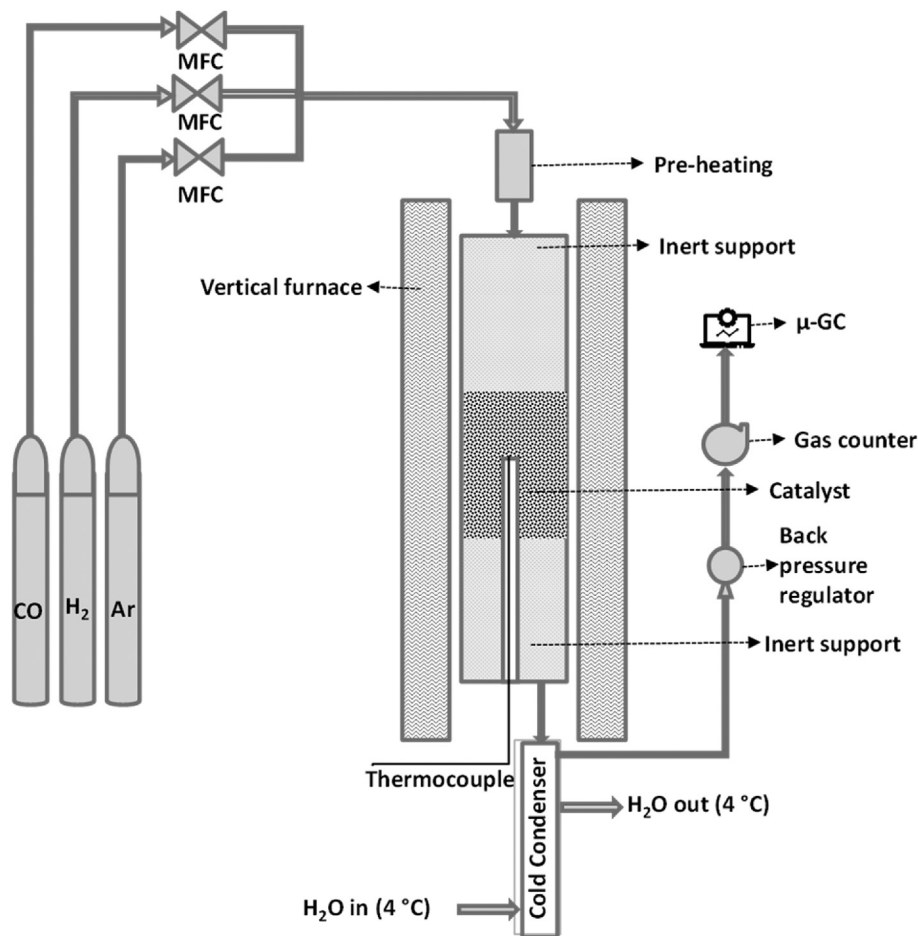


**Fig. 1 – Schematic diagram of the fixed-bed reactor.**

**Table 2.** The trend was similar to that observed from XRD analysis, i.e.  $\text{Co}_3\text{O}_4$  particle size on HAP ( $9.4 \pm 2.9$  nm) was consistently larger with broad distribution than on alumina ( $5.5 \pm 2.7$  nm). The deviation between the XRD and TEM techniques can be explained by the fact that XRD being a technique investigates crystallite sizes rather than particle sizes imaged from TEM technique [33]. The representative HAADF-STEM images of calcined Co/HAP and Co/Alumina catalysts are depicted in Fig. 3.  $\text{Co}_3\text{O}_4$  particles were relatively well dispersed on both the supports, however, Co/Alumina catalysts contain very small particles ( $\sim 2\text{--}3$  nm, Fig. 3d) that often occur in clusters. The cobalt oxide particles and their distribution were identified and assessed by imaging the main elements with an EDX analyzer (Figs. S4–6). The histogram of  $\text{Co}_3\text{O}_4$  particle size clearly shows that very negligible percentage of particles present below 5–6 nm on Co/HAP, whereas, significant percentage (about 50%) of particles exist in this range on Co/Alumina (Fig. 4). Such small cobalt oxide particles are generally very hard to reduce during the *in-situ* catalyst reduction step that precedes the FT catalytic test.

The reduction behavior of both Co/HAP and Co/Alumina catalysts was studied using TPR measurements (Fig. 5). The TPR results showed that  $\text{Co}_3\text{O}_4$  particles on both the catalysts exhibited the typical two-step reduction pattern: i.e. in the step I)  $\text{Co}_3\text{O}_4$  is reduced to CoO, and in the step II) CoO is reduced to metallic cobalt. The use of HAP as support for

cobalt precursor has shifted the reduction temperature of step I to  $\sim 350$  °C from  $\sim 380$  °C on alumina support. Further, the step II on HAP reached maximum reduction at  $\sim 540$  °C and was almost completed by 750 °C, owing to the absence of small cobalt oxide particles which correlates well the particle size distribution obtained from TEM analysis. However, on alumina support step II of cobalt reduction process takes place very slowly and reduction is not even complete at 1000 °C, due to the presence of very small cobalt oxide particles that are generally very hard to reduce. In addition, alumina is also known to interact with cobalt oxides forming refractory Co-aluminate species which are also difficult to reduce. Thus, TPR results clearly shows the advantage of using HAP support to improve the reducibility of cobalt oxide species compared to alumina support.

#### **Catalytic performance of Co/HAP and Co/Alumina in FT synthesis**

Co/HAP catalysts reduced *in-situ* at 350 °C for 7 h were tested in FT synthesis under different reaction conditions to evaluate and compare its catalytic efficiency with Co/Alumina catalysts. The results depicted in Fig. 6 show that using Co/HAP catalysts, CO conversions were consistently higher when compared to Co/Alumina catalysts under different GHSV and reaction temperatures. CO conversions of about 85% were

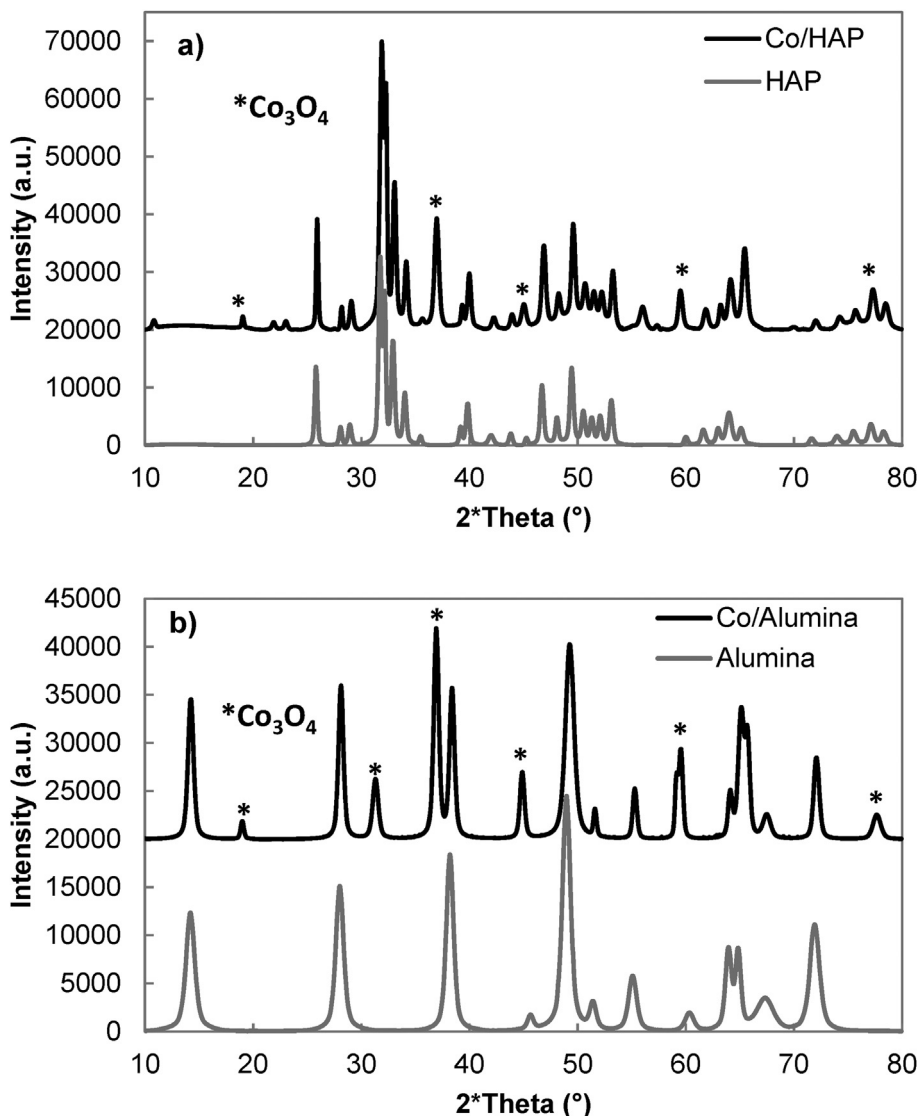


Fig. 2 – XRD patterns of the supports and the catalysts, a) HAP and Co/HAP; b) Alumina and Co/Alumina.

achieved using Co/HAP catalysts, whereas, under similar conditions (GHSV: 770 mL g<sub>cat</sub><sup>-1</sup> h<sup>-1</sup>, 20 bar, 230 °C) Co/Alumina catalysts yielded only about 11% of CO conversion. Interestingly, the C<sub>5+</sub> selectivity for Co/HAP catalysts under different tested conditions remained at or above ~82% (Table 3), despite the very high CO conversions which might be attributed to the lower acid-site density of HAP support when compared to alumina support.

**Table 2 – Co<sub>3</sub>O<sub>4</sub> nanocrystallite size and average Co<sub>3</sub>O<sub>4</sub> particle size distribution in the calcined catalysts as measured from XRD and TEM analysis, respectively. Here, ± indicates the width of the distribution and not the uncertainty of the particle size.**

Catalysts	2*theta (36.9°) Co <sub>3</sub> O <sub>4</sub> (nm) – XRD	Average particle size (nm) – TEM
Co/HAP	12.2	9.4 ± 2.9
Co/Alumina	9.4	5.5 ± 2.7

Literature studies summarized in Table 4 show that increasing the cobalt loading from 8 to 15 wt% on alumina support, the CO conversions are at least doubled (i.e. from 11.6% to 22.0 or 49.5%) despite of the differences in textural properties of the catalyst and testing conditions. Direct comparison of the CO conversions in this study with those available in the literature is not straight forward due to the differences in the catalyst preparation and testing conditions. Nevertheless, the CO conversions on Co/Alumina obtained in this study is relatively low when compared those reported in the previous studies (Table 4), and this can be attributed to the presence of 50% cobalt crystallites in the range of 5–6 nm (from TEM analysis, Fig. 4 and Table 2). It has been established in the literature that Co particles <6 nm exhibit lower intrinsic activity when compared to larger Co particles >6 nm [34]. Further, the TPR profile of Co/Alumina in this study exhibited a broad peak above 900 °C with maximum at 1000 °C which is generally attributed to the presence nonreducible and catalytically inactive Co aluminate species [35]. Consequently, explaining the low catalytic activity of Co/Alumina. The

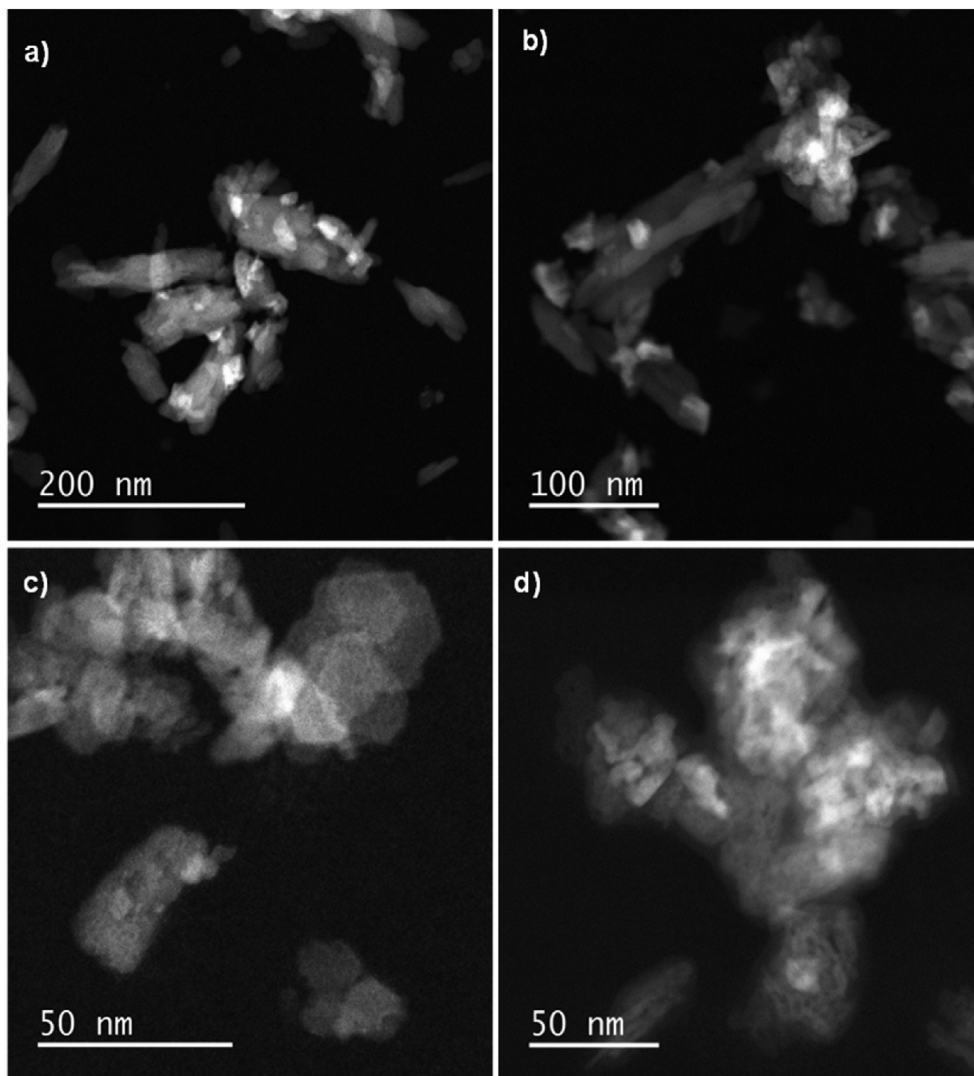


Fig. 3 – HAADF-STEM images of calcined catalysts: a–b) Co/HAP and c–d) Co/Alumina.

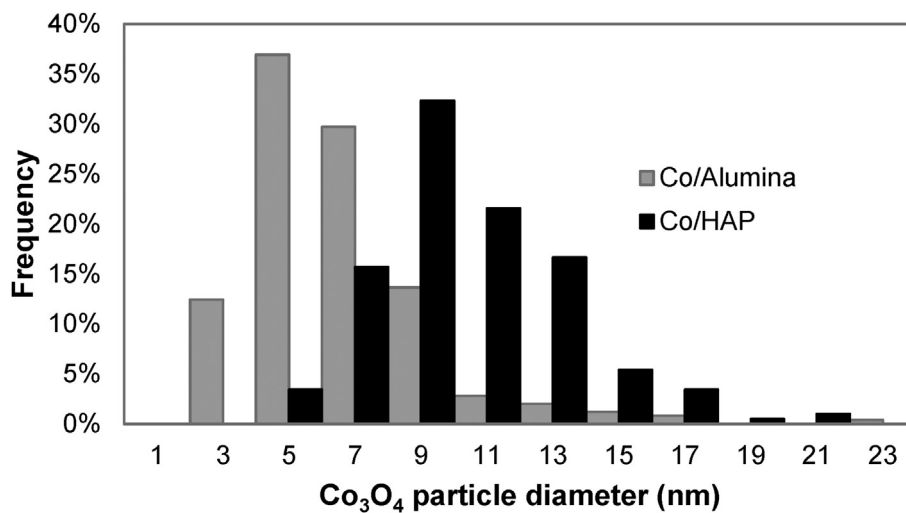


Fig. 4 – Co<sub>3</sub>O<sub>4</sub> particle size distribution in calcined catalysts; Co/HAP and Co/Alumina.



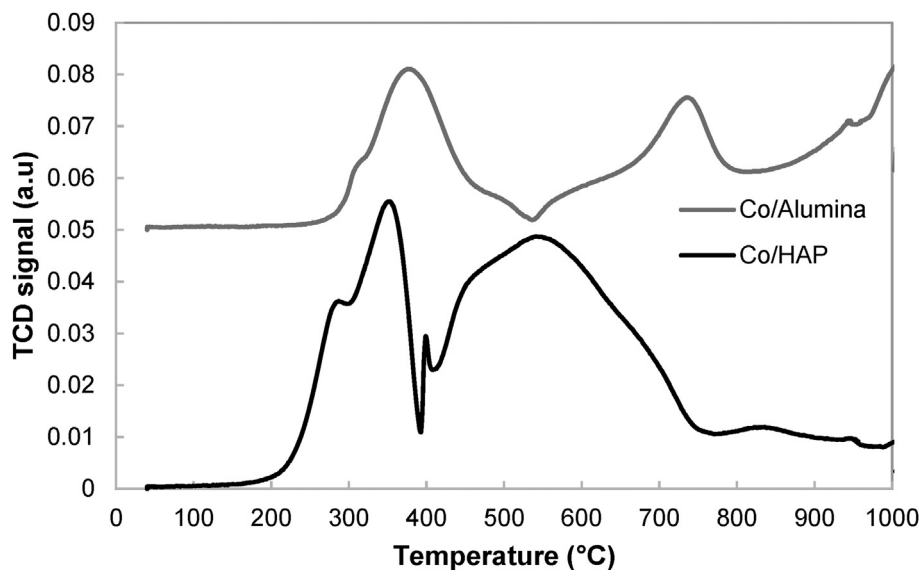


Fig. 5 – TPR profiles for Co/HAP and Co/Alumina catalysts.

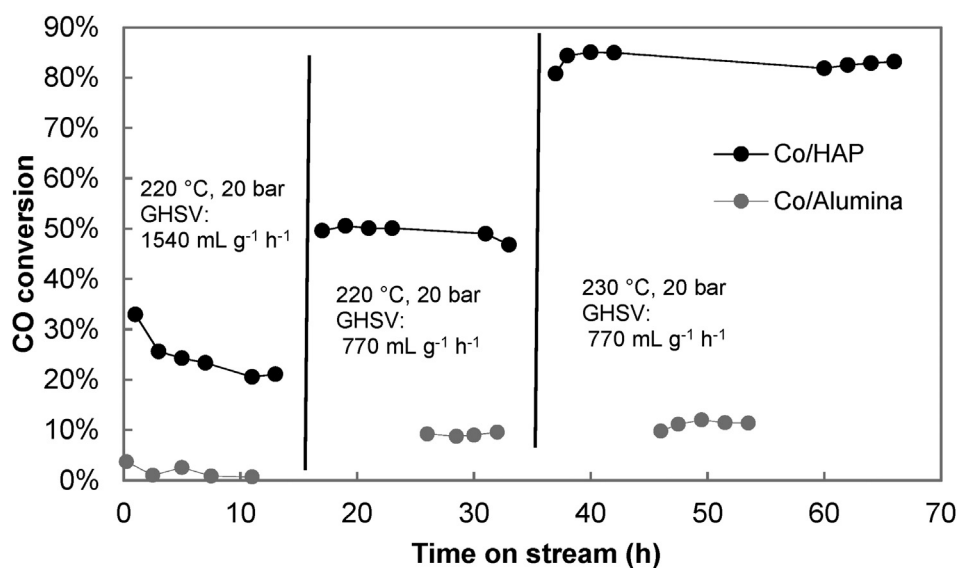


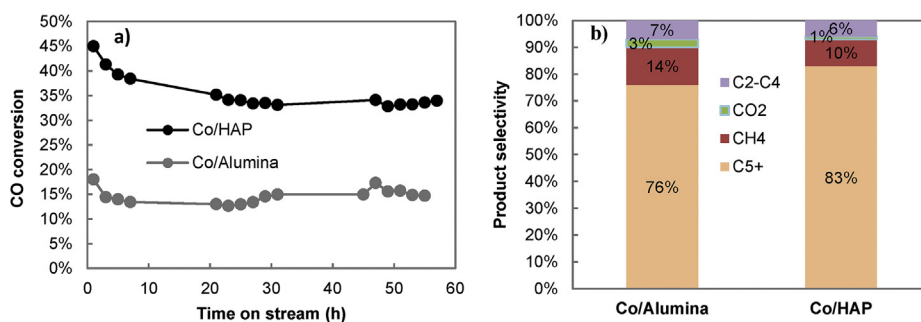
Fig. 6 – CO conversions in FT synthesis using Co/HAP and Co/Alumina catalysts reduced at 350 °C under reactions conditions of 20 bar pressure with different gas hourly space velocities (GHSV: 1540 or 770 mL g<sup>-1</sup> h<sup>-1</sup>) and temperatures (220 or 230 °C).

Table 3 – FT product selectivity of Co/HAP and Co/Alumina catalysts reduced at 350 °C under different reaction conditions at 20 bar pressure. Temp. represents temperature, Sel. represents selectivity.

Catalyst	Temp. °C	GHSV mL g <sup>-1</sup> h <sup>-1</sup>	CO Conversion %	Sel. CH <sub>4</sub> %	Sel. CO <sub>2</sub> %	Sel. C <sub>2-4</sub> %	Sel. C <sub>5+</sub> %
Co/HAP	220	1540	~22	~11	~1	~5	~83
	220	770	~50	~9	~1	~4	~86
	230	770	~83	~11	~2	~5	~82
Co/Alumina	220	1540	~4	–	–	–	–
	220	770	~9	~5	~4	~2	~88
	230	770	~11	~8	~6	~4	~82

**Table 4 – CO conversion and product selectivity of Co/ $\gamma$ -Al<sub>2</sub>O<sub>3</sub> catalysts with different cobalt loading reported in the literature. Catalyst reduction temperature was 400 °C for all the catalysts with reduction time ranging from 6 to 18 h. FTS Temp. represents FT synthesis temperature; Wt. represents weight; dCo<sub>3</sub>O<sub>4</sub> represents crystallite diameter from XRD analysis; Red. Temp represents catalyst reduction temperature; and Conv. represents conversion. \*GHSV unit is h<sup>-1</sup>.**

Catalyst	SA <sub>BET</sub> m <sup>2</sup> g <sup>-1</sup>	Co wt. %	dCo <sub>3</sub> O <sub>4</sub> nm	FTS Temp. °C	Pressure bar	H <sub>2</sub> /CO	GHSV mL g <sup>-1</sup> h <sup>-1</sup>	CO conv. %	Ref.
Co/ $\gamma$ -Al <sub>2</sub> O <sub>3</sub>	165	8	9.6	212	20	2	5000*	11.6	[37]
Co/ $\gamma$ -Al <sub>2</sub> O <sub>3</sub>	235	12	15.0	220	20	2	500	33.1	[38]
Co/ $\gamma$ -Al <sub>2</sub> O <sub>3</sub>	159	15	12.4	212	20	2	5000*	22.0	[39]
Co/ $\gamma$ -Al <sub>2</sub> O <sub>3</sub>	221	15	10.1	230	28	2	1000	49.5	[40]



**Fig. 7 – a) CO conversions and b) product selectivity in FT synthesis using Co/HAP and Co/Alumina catalysts reduced at 400 °C under reactions conditions of 20 bar pressure with a gas hourly space velocity (GHSV) of 770 mL g<sup>-1</sup> h<sup>-1</sup> and 220 °C temperature.**

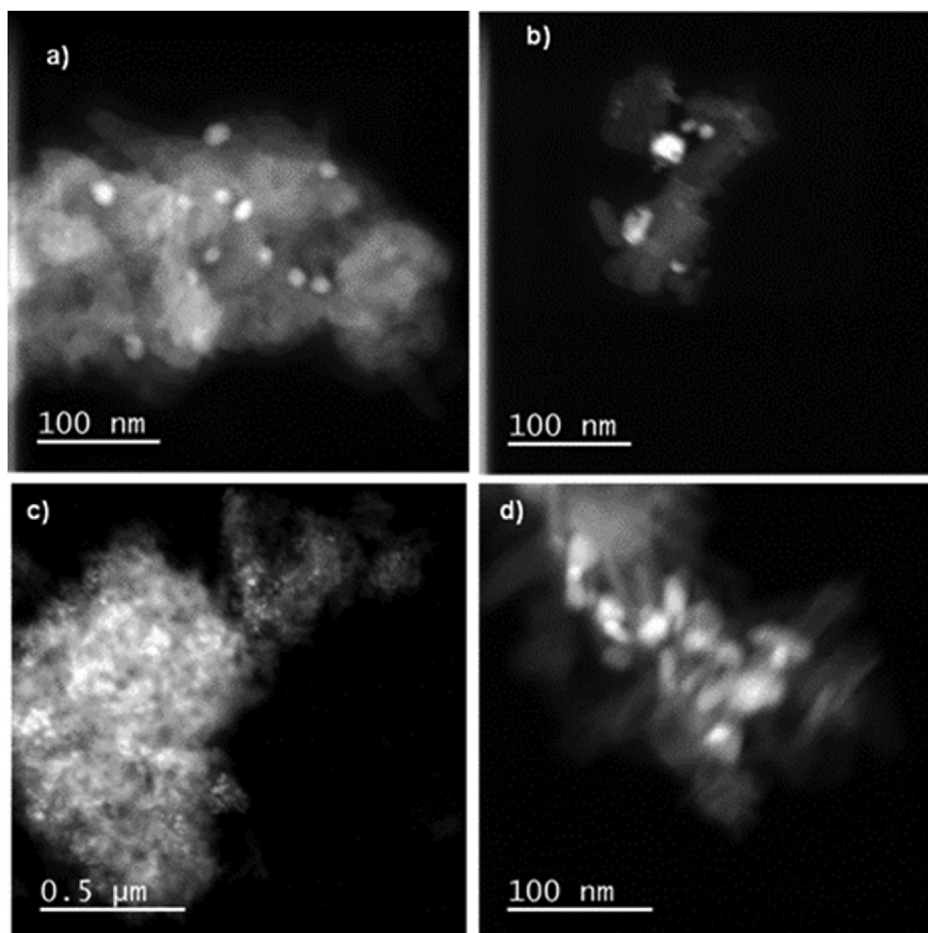


**Fig. 8 – HAADF-STEM images of the Co/HAP catalysts tested in FT synthesis that were reduced at 350 °C (images a-b) and 400 °C (images c-d).**

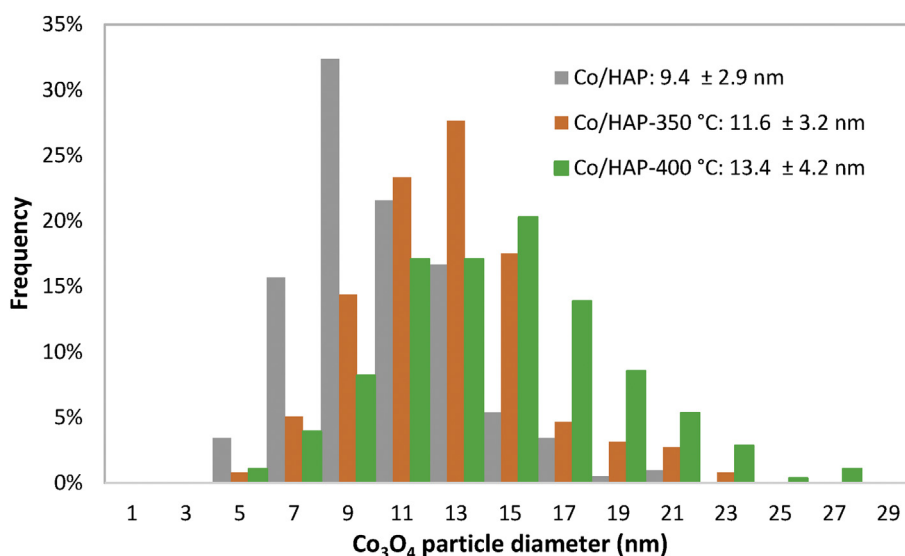


**Fig. 9** – Cobalt particle size distribution of Co/HAP calcined catalyst at 350 °C (Co/HAP) and Co/HAP catalysts tested in FT synthesis that were reduced at 350 °C (Co/HAP-350 °C) and 400 °C (Co/HAP-400 °C). The average value of the particle sizes for these catalysts obtained from the statistical treatment of TEM images are given in the legend.

optimum activity for Co/Alumina was reported to be at 12 wt% loading, because the increase in Co loading favors the readily reducible Co<sub>3</sub>O<sub>4</sub> and the high-temperature peak (>900 °C) in TPR analysis shifts to lower temperature [35]. As a result, commercial Co/Alumina catalysts contain cobalt loading of 12 to 30 wt% along with promoters such as Re (~0.5 wt%) or Pt (0.05 wt%) which significantly enhances the reducibility of cobalt [36].

Next, the *in-situ* reduction temperature and reduction time of the catalysts were increased from 350 °C to 400 °C and from 7 h to 16 h, respectively, to study its effect on catalytic performance. This might help in increasing the reducibility of Co/Alumina catalyst. As depicted in Fig. 7, the CO conversions (35%) using Co/HAP were still better than its alumina counterpart (15%). Co/HAP catalyst exhibited very good C<sub>5+</sub> selectivity (~83%) with low methane selectivity (10%). However, Co/Alumina catalyst displayed low C<sub>5+</sub> selectivity (73%) and relatively higher methane selectivity (14%) even at low CO conversion.

As expected, the CO conversions were slightly increased (15% versus 9%) by increasing the reduction temperature from 350 °C to 400 °C for Co/Alumina catalysts. However, the CO conversions over Co/HAP catalysts dropped from 50% to 35%. This prompted us to evaluate the Co particle size on tested Co/HAP catalysts reduced at 350 °C and 400 °C in TEM analysis (Fig. 8). The histogram of Co/HAP reduced at 400 °C and tested in FT synthesis showed larger Co particle size and broader distribution width (13.4 ± 4.2 nm versus 11.6 ± 3.2 nm) compared to its counterpart reduced at 350 °C (Fig. 9). Increasing the reduction temperature and reduction time resulted in sintering of Co particles (Fig. 8), thus decreasing the number of active sites and consequently, explaining the decreased catalytic efficiency. In case of HAP support, there are no strong metal support interactions as generally observed in the case of alumina support resulting in sintering of active phase during thermal treatment at higher temperatures. Therefore, the increased catalytic efficiency of Co/HAP

catalysts are attributed to the better reducibility of cobalt precursors and absence of relatively small and hard to reduce cobalt oxide precursors.

## Conclusions

For the first time, HAP-supported cobalt catalysts were prepared, characterized and evaluated in FT synthesis. In general, irrespective of the tested reaction conditions, the Co/HAP catalysts with similar cobalt loading showed superior performance over its alumina counterparts in FT synthesis. Further, the selectivity to long-chain hydrocarbons was consistently higher than 82% and selectivity to methane was about 10%. The better catalytic efficiency was attributed to the facile reducibility of cobalt precursors over HAP support and absence of small and hard to reduce cobalt oxide species. Overall, HAP support proved to be promising material to support FT catalysts. As a logical extension of this study, the effect of tuning acid-basic character of HAP over the catalytic performance in FT synthesis is presently being investigated to evaluate its full potential.

## Acknowledgements

The authors gratefully acknowledge the technical help rendered by the staff members at the RAPSODEE center (CNRS UMR 5302). Maria-Teresa Hungria-Hernandez is thanked for TEM measurements.

## REFERENCES

- [1] Van De Loosdrecht J, Ciobica IM, Gibson P, Govender NS, Moodley DJ, Saib AM, et al. Providing fundamental and applied insights into Fischer-Tropsch catalysis: Sasol-Eindhoven University of Technology collaboration. *ACS Catal* 2016;6:3840–55. <https://doi.org/10.1021/acscatal.6b00595>.
- [2] Khodakov AY, Chu W, Fongarland P. Advances in the development of novel cobalt Fischer-Tropsch catalysts for synthesis of long-chain hydrocarbons and clean fuels. *Chem Rev* 2007;107:1692–744. <https://doi.org/10.1021/cr050972v>.
- [3] Jun Z, Shuzhong W, Zhiqiang W, Haiyu M, Lin C. Hydrogen-rich syngas produced from the co-pyrolysis of municipal solid waste and wheat straw. *Int J Hydrogen Energy* 2017;42:19701–8. <https://doi.org/10.1016/j.ijhydene.2017.06.166>.
- [4] Maisano S, Urbani F, Cipiti F, Freni F, Chiodo V. Syngas production by BFB gasification: experimental comparison of different biomasses. *Int J Hydrogen Energy* 2019;44:4414–22. <https://doi.org/10.1016/j.ijhydene.2018.11.148>.
- [5] Ail SS, Dasappa S. Biomass to liquid transportation fuel via Fischer Tropsch synthesis - Technology review and current scenario. *Renew Sustain Energy Rev* 2016;58:267–86. <https://doi.org/10.1016/j.rser.2015.12.143>.
- [6] Jahangiri H, Bennett J, Mahjoubi P, Wilson K, Gu S. A review of advanced catalyst development for Fischer-Tropsch synthesis of hydrocarbons from biomass derived syn-gas. *Catal Sci Technol* 2014;4:2210–29. <https://doi.org/10.1039/C4CY00327F>.
- [7] Khodakov AY. Fischer-Tropsch synthesis: relations between structure of cobalt catalysts and their catalytic performance. *Catal Today* 2009;144:251–7. <https://doi.org/10.1016/j.cattod.2008.10.036>.
- [8] de Smit E, Weckhuysen BM. The renaissance of iron-based Fischer-Tropsch synthesis: on the multifaceted catalyst deactivation behaviour. *Chem Soc Rev* 2008;37:2758. <https://doi.org/10.1039/b805427d>.
- [9] Munnik P, De Jongh PE, De Jong KP. Recent developments in the synthesis of supported catalysts. *Chem Rev* 2015;115:6687–718. <https://doi.org/10.1021/cr500486u>.
- [10] Prieto G, De Mello MIS, Concepción P, Murciano R, Pergher SBC, Martínez A. Cobalt-catalyzed Fischer-Tropsch synthesis: chemical nature of the oxide support as a performance descriptor. *ACS Catal* 2015;5:3323–35. <https://doi.org/10.1021/acscatal.5b00057>.
- [11] Munirathinam R, Pham Minh D, Nzihou A. Effect of the support and its surface modifications in cobalt-based Fischer-Tropsch synthesis. *Ind Eng Chem Res* 2018;57:16137–61. <https://doi.org/10.1021/acs.iecr.8b03850>.
- [12] Bartholomew CH, Reuel RC. Cobalt-support interactions: their effects on adsorption and CO hydrogenation activity and selectivity properties. *Ind Eng Chem Prod Res Dev* 1985;24:56–61. <https://doi.org/10.1021/i300017a011>.
- [13] Jiang ZS, Zhao YH, Huang CF, Song YH, Li DP, Liu ZT, et al. Metal-support interactions regulated via carbon coating – a case study of Co/SiO<sub>2</sub> for Fischer-Tropsch synthesis. *Fuel* 2018;226:213–20. <https://doi.org/10.1016/j.fuel.2018.03.195>.
- [14] Taghavi S, Tavasoli A, Asghari A, Signoretto M. Loading and promoter effects on the performance of nitrogen functionalized graphene nanosheets supported cobalt Fischer-Tropsch synthesis catalysts. *Int J Hydrogen Energy* 2019;44:10604–15. <https://doi.org/10.1016/j.ijhydene.2019.03.015>.
- [15] Morales BYF, Weckhuysen BM. Promotion effects in Co-based Fischer-Tropsch catalysis. *Catalysis* 2006;19:1–40. <https://doi.org/10.1039/9781847555229-00001>.
- [16] Khodakov AY, Griboval-Constant A, Bechara R, Zholobenko VL. Pore size effects in Fischer Tropsch synthesis over cobalt-supported mesoporous silicas. *J Catal* 2002;206:230–41. <https://doi.org/10.1006/jcat.2001.3496>.
- [17] González O, Pérez H, Navarro P, Almeida LC, Pacheco JG, Montes M. Use of different mesostructured materials based on silica as cobalt supports for the Fischer-Tropsch synthesis. *Catal Today* 2010;148:140–7. <https://doi.org/10.1016/j.cattod.2009.03.030>.
- [18] Udaya V, Rao S, Gormley RJ. Bifunctional catalysis in syngas conversions. *Catal Today* 1990;6:207–34. [https://doi.org/10.1016/0920-5861\(90\)85003-7](https://doi.org/10.1016/0920-5861(90)85003-7).
- [19] Bessell S. Investigation of bifunctional zeolite supported cobalt Fischer-Tropsch catalysts. *Appl Catal A Gen* 1995;126:235–44. [https://doi.org/10.1016/0926-860X\(95\)00040-2](https://doi.org/10.1016/0926-860X(95)00040-2).
- [20] Liu Y, Ersen O, Meny C, Luck F, Pham-Huu C. Fischer-Tropsch reaction on a thermally conductive and reusable silicon carbide support. *ChemSusChem* 2014;7:1218–39. <https://doi.org/10.1002/cssc.201300921>.
- [21] Lacroix M, Dreibine L, De Tymowski B, Vigneron F, Edouard D, Bégin D, et al. Silicon carbide foam composite containing cobalt as a highly selective and re-usable Fischer-Tropsch synthesis catalyst. *Appl Catal A Gen* 2011;397:62–72. <https://doi.org/10.1016/j.apcata.2011.02.012>.
- [22] Fihri A, Len C, Varma RS, Solhy A. Hydroxyapatite: a review of syntheses, structure and applications in heterogeneous catalysis. *Coord Chem Rev* 2017;347:48–76. <https://doi.org/10.1016/j.ccr.2017.06.009>.
- [23] Boukha Z, Kacimi M, Ziyad M, Ensuque A, Bozon-Verduraz F. Comparative study of catalytic activity of Pd loaded hydroxyapatite and fluoroapatite in butan-2-ol conversion and methane oxidation. *J Mol Catal A Chem* 2007;270:205–13. <https://doi.org/10.1016/j.molcata.2007.01.048>.
- [24] Boukha Z, Kacimi M, Pereira MFR, Faria JL, Figueiredo JL, Ziyad M. Methane dry reforming on Ni loaded hydroxyapatite and fluoroapatite. *Appl Catal A Gen* 2007;317:299–309. <https://doi.org/10.1016/j.apcata.2006.10.029>.
- [25] Tsuchida T, Kubo J, Yoshioka T, Sakuma S, Takeguchi T, Ueda W. Reaction of ethanol over hydroxyapatite affected by Ca/P ratio of catalyst. *J Catal* 2008;259:183–9. <https://doi.org/10.1016/j.jcat.2008.08.005>.
- [26] Silvester L, Lamonier J-F, Vannier R-N, Lamonier C, Capron M, Mamede A-S, et al. Structural, textural and acid-base properties of carbonate-containing hydroxyapatites. *J Mater Chem A* 2014;2:11073–90. <https://doi.org/10.1039/C4TA01628A>.
- [27] Boanini E, Gazzano M, Bigi A. Ionic substitutions in calcium phosphates synthesized at low temperature. *Acta Biomater* 2010;6:1882–94. <https://doi.org/10.1016/j.actbio.2009.12.041>.
- [28] Verwilghen C, Rio S, Nzihou A, Gauthier D, Flamant G, Sharrock PJ. Preparation of high specific surface area hydroxyapatite for environmental applications. *J Mater Sci* 2007;42:6062–6. <https://doi.org/10.1007/s10853-006-1160-y>.
- [29] Pham Minh D, Tran ND, Nzihou A, Sharrock P. One-step synthesis of calcium hydroxyapatite from calcium carbonate and orthophosphoric acid under moderate conditions. *Ind Eng Chem Res* 2013;52:1439–47. <https://doi.org/10.1021/ie302422d>.
- [30] Galera Martínez M, Pham Minh D, Weiss-Hortala E, Nzihou A, Sharrock P. Synthesis, characterization, and thermo-mechanical properties of copper-loaded apatitic calcium phosphates. *Compos Interfaces* 2013;20:647–60. <https://doi.org/10.1080/15685543.2013.834208>.
- [31] Phan TS, Sane AR, Rêgo de Vasconcelos B, Nzihou A, Sharrock P, Grouset D, et al. Hydroxyapatite supported bimetallic cobalt and nickel catalysts for syngas production

- from dry reforming of methane. *Appl Catal B Environ* 2018;224:310–21. <https://doi.org/10.1016/j.apcatb.2017.10.063>.
- [32] Rêgo de Vasconcelos B, Pham Minh D, Sharrock P, Nzihou A. Regeneration study of Ni/hydroxyapatite spent catalyst from dry reforming. *Catal Today* 2018;310:107–15. <https://doi.org/10.1016/j.cattod.2017.05.092>.
- [33] Eschemann TO, Oenema J, De Jong KP. Effects of noble metal promotion for Co/TiO<sub>2</sub> Fischer-Tropsch catalysts. *Catal Today* 2016;261:60–6. <https://doi.org/10.1016/j.cattod.2015.06.016>.
- [34] Den Breejen JP, Radstake PB, Bezemer GL, Bitter JH, Frøseth V, Holmen A, et al. On the origin of the cobalt particle size effects in. *J Am Chem Soc* 2009;131:7197–203. <https://doi.org/10.1016/j.cattod.2008.10.036>.
- [35] Wang WJ, Chen YW. Influence of metal loading on the reducibility and hydrogenation activity of cobalt/alumina catalysts. *Appl Catal* 1991;77:223–33. [https://doi.org/10.1016/0166-9834\(91\)80067-7](https://doi.org/10.1016/0166-9834(91)80067-7).
- [36] Rytter E, Holmen A. Deactivation and regeneration of commercial Type Fischer-Tropsch Co-Catalysts—a mini-review. *Catalysts* 2015;5:478–99. <https://doi.org/10.3390/catal5020478>.
- [37] Jean-Marie A, Griboval-Constant A, Khodakov AY, Diehl F. Influence of sub-stoichiometric sorbitol addition modes on the structure and catalytic performance of alumina-supported cobalt Fischer-Tropsch catalysts. *Catal Today* 2011;171:180–5. <https://doi.org/10.1016/j.cattod.2011.04.002>.
- [38] Zhang J, Chen J, Ren J, Li Y, Sun Y. Support effect of Co/Al<sub>2</sub>O<sub>3</sub> catalysts for Fischer-Tropsch synthesis. *Fuel* 2003;82:581–6. [https://doi.org/10.1016/S0016-2361\(02\)00331-9](https://doi.org/10.1016/S0016-2361(02)00331-9).
- [39] Jean-Marie A, Griboval-Constant A, Khodakov AY, Diehl F. Cobalt supported on alumina and silica-doped alumina: catalyst structure and catalytic performance in Fischer-Tropsch synthesis. *Comptes Rendus Chim* 2009;12:660–7. <https://doi.org/10.1016/j.crci.2008.07.008>.
- [40] Vosoughi V, Badoga S, Dalai AK, Abatzoglou N. Modification of mesoporous alumina as a support for cobalt-based catalyst in Fischer-Tropsch synthesis. *Fuel Process Technol* 2017;162:55–65. <https://doi.org/10.1016/j.fuproc.2017.03.029>.